

Highlights

Kinematic Guidance using Virtual Reference Point for Underactuated Marine Vehicles with Sideslip Compensation

S.K Mallipeddi, M. Menghini, S. Simani, P. Castaldi

- Kinematic guidance using Virtual Reference Point(VRP) for underactuated marine vehicles .
- Controlled Lyapunov function based Model Predictive Controller (MPC) to have optimal response between cross tracking error and heading error.
- Integration adaptive extended Kalman filter like observer with MPC to compensate for the sideslip due to ocean currents.

Kinematic Guidance using Virtual Reference Point for Underactuated Marine Vehicles with Sideslip Compensation

S.K Mallipeddi^{a,*}, M. Menghini^a, S. Simani^b and P. Castaldi^a

^aDepartment of Electrical, Electronic and Information Engineering (DEI) "Guglielmo Marconi", University of Bologna, Viale Risorgimento 2, Bologna, 40136, Italy

^bDepartment of engineering, University of Ferrara, Via Savonarola, 9, Ferrara, 44121, Italy

ARTICLE INFO

Keywords:

Underactuated Marine Vehicles.
Line of Sight.
Virtual Reference Point.
Guidance.
Model Predictive Control (MPC).

ABSTRACT

Path following for underwater vehicles remains a significant challenge due to underactuation in the sway and heave directions. Most existing approaches rely on line-of-sight guidance to address this issue. In this paper, we explore an alternative approach using kinematic guidance, based on virtual reference point guidance, wherein a fictitious point offset from the vehicle's center of rotation is used to reformulate the kinematic control problem and mitigate underactuation constraints. While this concept has been explored to some extent, previous works have largely overlooked the impact of the vehicle's attitude. To address this limitation, we propose a solution that simultaneously accounts for the vehicle's attitude while minimizing cross-track error by defining the error dynamics in the body reference frame, which enables direct control of yaw and sway through yaw rate actuation. A model predictive controller is designed to optimize both attitude stabilization and trajectory tracking performance and is enhanced with an adaptive extended Kalman filter-like observer to estimate the sideslip caused by ocean currents and external disturbances. The proposed controller is evaluated under the influence of ocean currents and modeling uncertainties, and compared to an existing method from the literature, demonstrating its effectiveness in maintaining path-following accuracy while stabilizing the attitude.

1. Introduction

Autonomous Marine Vehicles (AMVs) are increasingly vital as they allow for long-duration, high-risk, or repetitive tasks to be conducted without direct human presence, significantly reducing costs and increasing safety. AMVs include Autonomous Surface Vehicles (ASVs) and Autonomous Underwater Vehicles (AUVs) that perform various missions including oceanographic surveys [1], environmental monitoring [2], infrastructure inspection [3], search and rescue [4], and military operations [5]. Their autonomy enables exploration of hazardous or remote regions, such as deep-sea environments or areas affected by severe weather, that would otherwise be inaccessible. A common characteristic of many AMVs, especially those designed for practical and energy-efficient operations, is that they are underactuated, meaning they possess fewer control inputs than degrees of freedom that need to be controlled. This design choice often simplifies construction, reduces energy consumption, and improves endurance, but it also introduces substantial challenges for precise maneuvering and control [6].

This article focuses on a class of underactuated marine vehicles that operate primarily in the horizontal plane, such

as ASVs and AUVs, which maintain depth through dedicated depth controllers [7], with minimal pitching or vertical motion affecting their horizontal dynamics. The primary challenge for these vehicles lies in the path-following problem, where the objective is to ensure that the vehicle converges to and follows a predefined spatial path, independent of the time along that path [8]. This capability is essential for a wide range of missions, including systematic seabed mapping, pipeline or cable inspection, and environmental sampling, where spatial coverage and precision are critical. Path-following is particularly challenging for underactuated vehicles due to their limited control authority and the influence of external disturbances such as ocean currents [9].

To address the path-following problem in underactuated marine vehicles, various guidance laws have been proposed to generate desired headings that steer the vehicle along a predefined path. Among the most widely used are Line-of-Sight (LOS)-based methods [10, 11], which compute a desired heading that minimizes the cross-track error, typically using a scalar variable that parametrizes the path. These guidance commands result in yaw rotations that indirectly induce sway motion, thereby compensating for the lack of direct lateral actuation in underactuated systems. The Proportional LOS (PLOS) method introduces a look-ahead distance to improve stability, with a formulation allowing for uniform global stability proposed in [12]. Time-varying look-ahead distance strategies have also been developed to achieve better transient performance and compensate for external disturbances [13, 14].

However, PLOS may still exhibit steady-state errors under persistent disturbances such as constant ocean currents. To address this limitation, the Integral LOS (ILOS) method [15, 16] incorporates an integral term of the cross-track error

 sivakumar.mallipedd2@unibo.it (S.K Mallipeddi);
massimilian.menghin3@unibo.it (M. Menghini); silvio.simani@unife.it
(S. Simani); paolo.castaldi@unibo.it (P. Castaldi)
 <https://orcid.org/0009-0001-0182-1439> (S.K Mallipeddi);
www.unibo.it/sitoweb/massimilian.menghin3/en (M. Menghini);
<https://orcid.org/0000-0003-1815-2478> (S. Simani);
www.unibo.it/sitoweb/paolo.castaldi/en (P. Castaldi)
ORCID(s): 0009-0001-0182-1439 (S.K Mallipeddi);
0000-0001-8768-8984 (M. Menghini); 0000-0003-1815-2478 (S. Simani);
0000-0001-5754-5616 (P. Castaldi)

into the guidance law. This integral action allows the system to reject constant biases and ensures zero steady-state cross-track error [17]. In more advanced scenarios, Adaptive LOS (ALOS) strategies [18, 19] integrate real-time estimates of sideslip angles are used in the guidance computation. These methods have been shown to achieve uniform semi-global stability [18]. However, the performance of ALOS depends on the tuning of the adaptation gain: while higher gains can improve convergence speed, they may also lead to undesirable oscillations during transient phases. To mitigate such issues, Extended State Observer-based LOS (ELOS) methods have been proposed [20]. ELOS leverages an observer framework to estimate both unmeasured states and disturbances, feeding this information back into the guidance system for real-time compensation. Compared to ILOS and ALOS, ELOS offers a more systematic and robust approach to disturbance rejection, particularly when facing complex or time-varying environmental conditions.

Beyond LOS-based approaches, vector field guidance strategies have gained attention for their ability to construct smooth vector fields that guide the vehicle toward the path using gradient-like behaviors [21]. A comparison between vector field and LOS guidance methods is presented in [22]. For a comprehensive review of recent advances in LOS guidance strategies, readers are referred to [23].

While most existing path-following approaches define the control objective relative to the vehicle's pivot point (center of rotation), an alternative concept found in the literature is the use of a Virtual Reference Point (VRP). The VRP is usually placed at the bow of the vehicle, ahead of the pivot point, and offers both theoretical and practical advantages. As demonstrated in [24, 25], selecting a forward-positioned VRP can have a naturally stabilizing effect on the guidance dynamics. This idea is analogous to the intuitive observation that pulling a trolley leads to more stable behavior than pushing it, as discussed in [26]. Beyond its stabilizing role, the VRP framework is advantageous in applications requiring sensor-driven navigation. For example, in seabed scanning or inspection tasks, sensors such as cameras or sonar are typically mounted at a location offset from the vehicle's center of rotation. By choosing the VRP to coincide with the sensor location, as suggested in [27], the guidance law can directly regulate the path of the sensor itself, enabling more accurate coverage and improving mission performance.

Another significant advantage of the VRP lies in its ability to help address the underactuation problem by leveraging the kinematic coupling introduced by the displacement between the VRP and the vehicle's pivot point. As illustrated conceptually in [28], let P denote the pivot point, and P_v denote the virtual reference point located a distance E ahead as shown in Figure 1. A surge force applied at P results in a corresponding motion at P_v in the surge direction. Similarly, applying a yaw torque around point P induces a sway component at P_v due to the offset E . This coupling effect allows sway-like actuation to emerge from the available inputs—despite the vehicle being underactuated. This

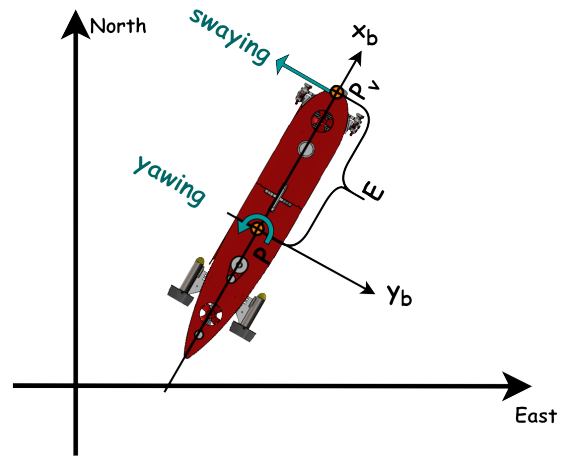


Figure 1: Schematic representation of the VRP located ahead of the pivot point by a distance E , introducing kinematic coupling between yaw and sway motions in underactuated marine vehicles

concept has been further explored in [29], where a control-oriented "handy matrix" formulation is proposed to map available actuation to the dynamics at the VRP, effectively exploiting this coupling to overcome underactuation. However, this mapping may yield multiple solutions, not all of which are physically meaningful or robust for control, as discussed in [30]. Moreover, using the VRP enables the vehicle's kinematics to be modeled similarly to nonholonomic systems, thus allowing the application of a wide range of nonlinear control strategies developed for such systems. For example, output feedback linearization can be employed by selecting the VRP as the output point, as demonstrated in [28, 27, 30]. This modeling approach not only enhances controllability but also integrates naturally with perception-driven navigation tasks.

To the best of the authors' knowledge, existing literature on guidance of underactuated AMVs using VRP guidance has primarily focused on the path-following problem, without explicitly addressing attitude tracking. In works such as [26, 29], the vehicle's attitude is assumed to remain stable due to the internal dynamics, but it is not regulated to follow a desired orientation. Similarly, in the output feedback linearization frameworks proposed in [28, 27, 30], the attitude dynamics are treated as internal and proven to be bounded, but not necessarily tracking a reference. In this work, we aim to bridge this gap by introducing a Nonlinear Model Predictive Control (NMPC) strategy that explicitly addresses both path-following and attitude regulation. The motivation for using an NMPC framework stems from the inherent kinematic coupling induced by the VRP, where sway and yaw motions are interdependent and influenced by a common set of control inputs. While previous approaches focused primarily on sway control and treated yaw behavior as a secondary or bounded effect, the proposed controller jointly optimizes both sway and yaw dynamics to achieve coordinated motion. Furthermore, we develop an Adaptive

Extended Kalman Filter (AEKF)-based observer to estimate the unknown sideslip angle, which is critical for accurate attitude tracking and compensation under environmental disturbances, such as ocean currents.

The remainder of this paper is organized as follows. Section 2 presents the dynamic model of the AMVs considered in this study. Section 3 formulates the path-following problem using the VRP framework. Section 4 describes the design of the AEKF observer used to estimate the sideslip angle. Section 5 details the two-loop control strategy—comprising the guidance and control loops—with a primary focus on the NMPC. Section 6 provides simulation results demonstrating the effectiveness of the proposed method under ocean current conditions, using the a AUV called "Blucy" as a case study. Finally, Section 7 concludes the paper and outlines directions for future work.

2. Vehicle Model

In this study, we consider a planar three-degree-of-freedom (3-DOF) model [31], suitable for a class of AUVs and ASVs that predominantly move in the horizontal plane. Vertical dynamics are excluded from this model under the assumption that they are either negligible or managed independently by a separate depth control system.

The vehicle's motion is defined in the North-East-Down (NED) inertial frame $\langle I \rangle$, where the position and orientation vector is given by $\eta = [x, y, \psi]^T \in \mathbb{R}^3$. The body-fixed velocity vector is $v = [u, v, r]^T \in \mathbb{R}^3$, representing surge, sway, and yaw rate, respectively. The rotation matrix that transforms velocities from the body frame $\langle b \rangle$ to the inertial frame is defined as:

$$J(\psi) = \begin{bmatrix} \cos \psi & -\sin \psi & 0 \\ \sin \psi & \cos \psi & 0 \\ 0 & 0 & 1 \end{bmatrix}, \quad J(\psi) \in SO(2) \quad (1)$$

where $SO(2)$ denotes the special orthogonal group of planar rotations.

The vehicle dynamics are described by the standard marine model as follows:

$$\dot{\eta} = J(\psi)v \quad (2a)$$

$$M\dot{v} + C(v)v + D(v)v = \tau_p + d(t) \quad (2b)$$

where $M \in \mathbb{R}^{3 \times 3}$ is the total inertia matrix composed of rigid-body inertia and added mass; $C(v)$ is the Coriolis-centripetal matrix including added mass effects; $D(v)$ is the hydrodynamic damping matrix, incorporating both linear and nonlinear terms; $\tau_p = [\tau_u, 0, \tau_r]^T \in \mathbb{R}^3$ is the control input vector; and $d(t) = [d_u, d_v, d_r]^T \in \mathbb{R}^3$ represents unknown environmental disturbances such as ocean currents and unmodeled dynamics. The absence of a control input in the sway direction reflects an underactuated configuration common in many marine vehicles.

To facilitate control design, we adopt the following assumptions:

Assumption 1. *The vehicle exhibits port-starboard symmetry, i.e., its dynamics are invariant under reflection about its longitudinal axis.*

Remark 1. This symmetry is typical of marine vehicles with streamlined hulls. It allows the neglect of certain off-diagonal terms in the added mass and damping matrices, simplifying the dynamic equations [31].

Assumption 2. *Hydrodynamic damping is considered to be linear with respect to the velocity of the Vehicle.*

Remark 2. Linear hydrodynamic damping is reasonable in low-speed operating conditions where nonlinear effects are minimal. Furthermore, the nonlinear damping terms, while neglected in this model, generally have a stabilizing effect, as they introduce energy dissipation that naturally enhances system stability.

Assumption 3. *The external disturbances $d(t)$ are bounded such that $|d_n| \leq \bar{d}_n$ for $n = u, v, r$, where \bar{d}_n are unknown but finite constants.*

Remark 3. This models real-world effects like current, wind, or wave-induced forces that, although uncertain, are naturally constrained by environmental limits.

Under Assumptions 1–3, and by resolving the vector-matrix equations into scalar components, the vehicle model can be reformulated as:

$$\dot{x} = u \cos \psi - v \sin \psi \quad (3a)$$

$$\dot{y} = u \sin \psi + v \cos \psi \quad (3b)$$

$$\dot{\psi} = r \quad (3c)$$

$$\dot{u} = F_u(u, v, r) + \tau_u + d_u \quad (4a)$$

$$\dot{v} = Y(u)v + X(u)r + d_v \quad (4b)$$

$$\dot{r} = F_r(u, v, r) + \tau_r + d_r \quad (4c)$$

where the functions F_u , F_r , $X(u)$, and $Y(u)$ are defined as:

$$\begin{aligned} F_u(u, v, r) &= \frac{1}{m_{11}}(m_{22}v + m_{23}r)r - \frac{d_{11}}{m_{11}}u \\ F_r(u, v, r) &= \frac{m_{23}d_{22} - m_{22}(d_{32} + (m_{22} - m_{11})u)}{m_{22}m_{33} - m_{23}^2}v \\ &\quad + \frac{m_{23}(d_{23} + m_{11}u) - m_{22}(d_{33} + m_{23}u)}{m_{22}m_{33} - m_{23}^2} \\ X_1 &= \frac{m_{11}m_{33} - m_{23}^2}{m_{22}m_{33} - m_{23}^2}, \quad X_2 = \frac{d_{33}m_{23} - d_{23}m_{33}}{m_{22}m_{33} - m_{23}^2} \\ Y_1 &= \frac{(m_{11} - m_{22})m_{23}}{m_{22}m_{33} - m_{23}^2}, \quad Y_2 = \frac{d_{22}m_{33} - d_{32}m_{23}}{m_{22}m_{33} - m_{23}^2} \\ X(u) &= -X_1u + X_2, \quad Y(u) = -Y_1u - Y_2 \end{aligned} \quad (5)$$

Here, m_{ij} and d_{ij} denote the entries of the inertia matrix M and the damping matrix D .

3. Problem Formulation

Let $P = [x, y]^T \in \mathbb{R}^2$ denote the position of the pivoting point expressed in the inertial frame $\langle I \rangle$. Traditionally, this point is used for path-following problems. In this study, the VRP, denoted by $P_v \in \mathbb{R}^2$, is used for path following. The relation between P and P_v is given by:

$$P_v = P + R(\psi)E \quad (6)$$

where $E = [E_x, E_y]^T \in \mathbb{R}^2$ represents the position vector from the pivoting point P to the virtual point P_v in body frame $\langle b \rangle$. It is chosen such that $E_x > 0$ and $E_y = 0$, placing the VRP at the bow of the vehicle. The matrix $R(\psi) \in SO(2)$ represents the rotation matrix from body to inertial frame and is expressed as:

$$R(\psi) = R = \begin{bmatrix} \cos \psi & -\sin \psi \\ \sin \psi & \cos \psi \end{bmatrix} \quad (7)$$

Consider a reference path \mathcal{P} parameterized as $P_d = [x_d(\zeta), y_d(\zeta)]^T \in \mathbb{R}^2$, with a scalar path variable $\zeta \in \mathbb{R}$ that moves along the path with velocity $U_d > 0$.

Assumption 4. *The reference path \mathcal{P} is smooth and at least twice differentiable (C^2) to ensure well-defined curvature and tangent vectors.*

Let the frame $\langle P \rangle$, referred to as the local path-tangent frame, is defined such that its x-axis is aligned with the tangent to the path at $P_d(\zeta)$ and its y-axis is normal to the path. This frame moves along the path with velocity U_d , and the variable ζ is updated according to:

$$\dot{\zeta} = \frac{U_d}{\sqrt{x_d'^2(\zeta) + y_d'^2(\zeta)}} \quad (8)$$

This ensures that the frame $\langle P \rangle$ continuously tracks the motion along the path, providing a convenient moving reference. The angle between this frame and inertial frame $\langle I \rangle$ is denoted by γ_d , and it is computed as:

$$\gamma_d = \text{atan2}(y_d'(\zeta), x_d'(\zeta)) \quad (9)$$

where $x_d'(\zeta) = \frac{dx_d}{d\zeta}$ and $y_d'(\zeta) = \frac{dy_d}{d\zeta}$. The associated rotation matrix $R_p(\gamma_d) \in SO(2)$ is given by:

$$R_p(\gamma_d) = R_p = \begin{bmatrix} \cos \gamma_d & -\sin \gamma_d \\ \sin \gamma_d & \cos \gamma_d \end{bmatrix} \quad (10)$$

The path-following error between the vehicle's VRP and the desired path, expressed in the body frame, is defined as:

$$\varepsilon = R(\psi)^T(P_d - P_v) \quad (11)$$

where $\varepsilon = [x_e, y_e]^T \in \mathbb{R}^2$, with x_e referred to as the along-track error and y_e as the cross-track error.

Taking the time derivative of ε , the error dynamics are given by:

$$\dot{\varepsilon} = \dot{R}^T(P_d - P_v) + R^T(\dot{P}_d - \dot{P}_v) \quad (12)$$

where:

$$\dot{R} = RS \quad (13)$$

and:

$$S = \begin{bmatrix} 0 & -\dot{\psi} \\ \dot{\psi} & 0 \end{bmatrix}, \quad \text{with } S = -S^T \quad (14)$$

The derivative of the desired path is:

$$\dot{P}_d = R_p \begin{bmatrix} U_d \\ 0 \end{bmatrix} \quad (15)$$

and:

$$\dot{P}_v = \dot{P} + \dot{R}E \quad (16)$$

From (3) and (13), the above equation can be rewritten as:

$$\dot{P}_v = R \begin{bmatrix} U \\ 0 \end{bmatrix} + RSE \quad (17)$$

where $U = \sqrt{u^2 + v^2}$ is the vehicle's resultant velocity. Substituting (13–17) into (12) yields:

$$\begin{aligned} \dot{\varepsilon} &= (RS)^T(P_d - P_v) + R^T \left(R_p \begin{bmatrix} U_d \\ 0 \end{bmatrix} - RS \begin{bmatrix} E_x \\ 0 \end{bmatrix} \right) \\ &= S^T \varepsilon + R^T R_p \begin{bmatrix} U_d \\ 0 \end{bmatrix} - S \begin{bmatrix} E_x \\ 0 \end{bmatrix} \end{aligned} \quad (18)$$

Expanding in scalar form:

$$\begin{aligned} \dot{x}_e &= U_d(\cos(\psi - \gamma_d) \cos \beta - \sin(\psi - \gamma_d) \sin \beta) \\ &\quad + \dot{\psi} y_e - U, \end{aligned} \quad (19a)$$

$$\begin{aligned} \dot{y}_e &= U_d(\sin(\psi - \gamma_d) \cos \beta + \cos(\psi - \gamma_d) \sin \beta) \\ &\quad - \dot{\psi} x_e - E_x r \end{aligned} \quad (19b)$$

The quantity $\beta = \text{atan2}(v, u)$ represents the sideslip angle, which arises from external disturbances or a non-zero sway velocity during a turn, causing a deviation in the vehicle's orientation ψ as explained in [32].

Assumption 5. *In this work, the sideslip angle β is assumed to be small, such that $\sin \beta \approx \beta$ and $\cos \beta \approx 1$.*

Under Assumption 5, equations (19) simplify to:

$$\dot{x}_e = U_d \cos(\psi - \gamma_d) - U_d \sin(\psi - \gamma_d)\beta + \dot{\psi} y_e - U \quad (20a)$$

$$\dot{y}_e = U_d \sin(\psi - \gamma_d) + U_d \cos(\psi - \gamma_d)\beta - \dot{\psi} x_e - E_x r \quad (20b)$$

The objective of the controller is to drive $x_e \rightarrow 0$ and $y_e \rightarrow 0$, aligning the vehicle's heading tangentially with the reference path. Accordingly, the desired heading ψ_d is defined as:

$$\psi_d = \gamma_d - \beta \quad (21)$$

Remark 4. Note that the sideslip angle β appears in both equations (20) and (21). However, β is an unknown quantity that must be estimated. Moreover, the attitude error dynamics $\dot{\psi}_e$ have not yet been explicitly addressed. These aspects will be discussed in the following sections.

4. Adaptive Observer Design

In this section, an AEKF-like observer is designed, inspired by [33] to estimate the sideslip angle β . Although the design procedure is identical, the considered dynamics differ slightly.

To construct the adaptive observer, equation (20) is rewritten in a state-affine form:

$$\dot{\varepsilon} = A(t)\varepsilon + \varphi(t) + \Phi(t)\beta \quad (22a)$$

$$y = C\varepsilon \quad (22b)$$

where $\varphi(t) = [U_d \cos(\psi - \gamma_d) - U, U_d \sin(\psi - \gamma_d) - E_x r]^T$, $\Phi(t) = [-U_d \sin(\psi - \gamma_d), U_d \cos(\psi - \gamma_d)]^T$, $C = I_{2 \times 2}$, and $A(t) = \begin{bmatrix} 0 & \gamma_d \\ -\gamma_d & 0 \end{bmatrix}$.

To ensure that the proposed AEKF observer accurately estimates the states and the sideslip angle β , the system is required to satisfy certain observability conditions. Specifically, the Uniform Observability Condition and the Persistent Excitation Condition are imposed.

Definition 1 (Uniform Observability Condition). [34] *The system (22) is said to satisfy uniform observability if there exist constants $0 < \alpha_1 < \sigma_1$ and $T_1 > 0$ such that:*

$$\alpha_1 I \leq \int_t^{t+T_1} \Psi(\tau)^T C^T \Sigma C \Psi(\tau) d\tau \leq \sigma_1 I, \quad \forall t \geq t_0 \quad (23)$$

for some $t_0 \geq 0$ and a bounded positive definite matrix Σ , where $\Psi(t)$ is the transition matrix of the system: $\dot{\varepsilon} = A(t)\varepsilon$, $y = C\varepsilon$.

Definition 2 (Persistent Excitation Condition). [34] *The function $\Phi(t)$ is said to be persistently exciting if there exists a vector function $\Lambda(t)$, which is a solution of $\dot{\Lambda} = [A(t) - K(t)C(t)]\Lambda + \Phi(t)$, where $K(t)$ is a time-varying feedback gain that stabilizes the system (22). The function $\Lambda(t)$ satisfies the persistence excitation condition if there exist constants $0 < \alpha_2 < \sigma_2$ and $T_2 > 0$ such that:*

$$\alpha_2 I \leq \int_t^{t+T_2} \Lambda(\tau)^T C^T \Sigma C \Lambda(\tau) d\tau \leq \sigma_2 I, \quad \forall t \geq t_0, \quad (24)$$

for some $t_0 \geq 0$ and a bounded positive definite matrix Σ .

Following [35] and [34], the AEKF is designed as follows:

$$\begin{aligned} \dot{\hat{\varepsilon}} &= A(t)\hat{\varepsilon} + \varphi(t) + \Phi(t)\hat{\beta} \\ &\quad + \left[\Lambda S_\beta^{-1} \Lambda^T C^T + S_\varepsilon^{-1} C^T \right] \Sigma (y - C\hat{\varepsilon}) \end{aligned} \quad (25a)$$

$$\dot{\hat{\beta}} = S_\beta^{-1} \Lambda^T C^T \Sigma (y - C\hat{\varepsilon}) \quad (25b)$$

$$\dot{\Lambda} = [A(t) - S_\varepsilon^{-1} C^T \Sigma C] \Lambda + \Phi(t) \quad (25c)$$

$$\dot{S}_\varepsilon = -\rho_\varepsilon S_\varepsilon - A(t)^T S_\varepsilon - S_\varepsilon A(t) + C^T \Sigma C, \quad S_\varepsilon(0) > 0 \quad (25d)$$

$$\dot{S}_\beta = -\rho_\beta S_\beta + \Lambda^T C^T \Sigma C \Lambda, \quad S_\beta(0) > 0 \quad (25e)$$

where $\hat{\varepsilon}$ and $\hat{\beta}$ denote the estimates of the tracking errors and the sideslip angle, respectively. The terms $\Lambda \in \mathbb{R}^2$, $S_\varepsilon \in \mathbb{R}^{2 \times 2}$, and $S_\beta \in \mathbb{R}$ are adaptive gains with adaptive laws (25c) - (25e). ρ_ε and ρ_β are sufficiently large constants. The matrix Σ is a bounded positive definite matrix.

By defining $\tilde{\varepsilon} = \hat{\varepsilon} - \varepsilon$ and $\tilde{\beta} = \hat{\beta} - \beta$, equations (25a) and (25b) can be written as:

$$\dot{\tilde{\varepsilon}} = \left(A(t) - \left[\Lambda S_\beta^{-1} \Lambda^T + S_\varepsilon \right] C^T \Sigma C \right) \tilde{\varepsilon} + \Phi(t) \tilde{\beta} \quad (26a)$$

$$\dot{\tilde{\beta}} = -S_\beta^{-1} \Lambda^T C^T \Sigma \tilde{\varepsilon} \quad (26b)$$

Remark 5. It can be verified that the considered system satisfies the conditions of uniform observability and persistence excitation. The function Ψ yields a rotation matrix, thus the term $\Psi^T C^T \Sigma C \Psi$ has the same eigenvalues as Σ . Since Σ is a bounded positive definite matrix the system satisfies the (23). The system (22), which is stabilized by $K = S_\varepsilon^{-1} C^T \Sigma C$, satisfies the upper bound of (24) since $\Phi(t)$ is bounded. For the lower bound, note that since the system is stable, $\dot{\Lambda} \approx \Phi$ for $t_0 > 0$. Since Φ is non zero at time $t > t_0$, Λ also remains nonzero. This ensures that $\Lambda^T C^T \Sigma C \Lambda$ remains positive definite, thereby satisfying the lower bound condition in (24).

Lemma 1. *Consider the adaptive observer defined by (25a) - (25e). If the system satisfies the Uniform Observability Condition (23) and the Persistent Excitation Condition (24), then the estimation errors $\tilde{\varepsilon} = \hat{\varepsilon} - \varepsilon$ and $\tilde{\beta} = \hat{\beta} - \beta$ are Uniformly Globally Exponentially Stable (UGES). Specifically, there exist positive constants $\sigma, \bar{\sigma}, \rho > 0$ such that:*

$$\|\tilde{\varepsilon}(t)\|^2 + |\tilde{\beta}(t)|^2 \leq \frac{\bar{\sigma}}{\sigma} e^{-\rho(t-t_0)} (\|\tilde{\varepsilon}(t_0)\|^2 + |\tilde{\beta}(t_0)|^2), \quad \forall t \geq t_0. \quad (27)$$

PROOF. Refer to [33] for a detailed proof.

The results of Lemma 1 can be expressed more compactly by defining $\zeta = [\tilde{\varepsilon}^T \tilde{\beta}]^T \in \mathbb{R}^3$, as follows:

$$\|\zeta(t)\| \leq \sqrt{\frac{\bar{\sigma}}{\sigma}} e^{-\frac{\rho}{2}(t-t_0)} \|\zeta(t_0)\| \quad (28)$$

This result establishes that the estimation errors $\tilde{\varepsilon}$ and $\tilde{\beta}$ decay exponentially to zero, ensuring the UGES of the adaptive observer. The rate of decay is governed by the parameter $\rho = \min(\rho_\varepsilon, \rho_\beta)$, which depends on the observer gains. The parameters σ and $\bar{\sigma}$ denote the smallest and largest singular values of the matrix $\text{diag}(S_\varepsilon, S_\beta)$. The ratio $\frac{\bar{\sigma}}{\sigma}$ quantifies how the initial estimation errors influence the convergence rate.

Theorem 1. *The observer error $\zeta(t)$ satisfy the exponential bound in (28) for all $t \geq t_0$, where $\rho > 0$ is the convergence rate and $\frac{\bar{\sigma}}{\sigma}$ is a positive constant.*

Then, for any $k_{\text{conv}} > 0$ and sampling time $\delta > 0$, there exists a maximum estimation error bound ζ_{max} such that:

$$\|\zeta(t)\| \leq \zeta_{\text{max}}, \quad \forall t \geq k_{\text{conv}} \delta, \quad (29)$$

where $k_{\text{conv}} > 0$ is a fixed number of sampling instants.

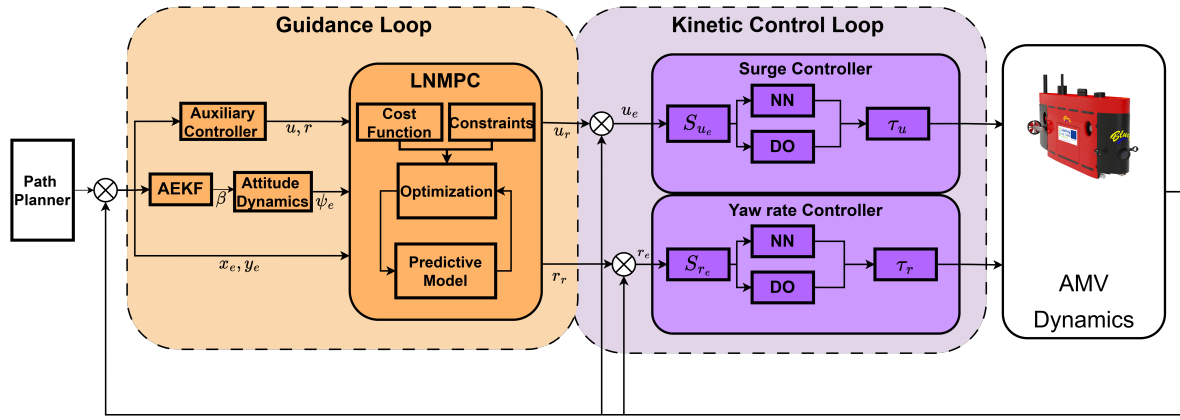


Figure 2: Block diagram of the proposed two-stage control architecture. The outer LNMPC based kinematic guidance loop generates reference signals for the inner surge and yaw rate controller.

PROOF. From Lemma 1, the observer error $\zeta(t)$ satisfies the exponential convergence bound as in (28). Fix any $k_{conv} > 0$ and sampling time $\delta > 0$, and consider that:

$$t = t_0 + k_{conv}\delta. \quad (30)$$

Substituting (30) into (28) yields the following expression:

$$\|\zeta(t_0 + k_{conv}\delta)\| \leq \sqrt{\frac{\sigma}{\sigma}} e^{-\frac{\rho}{2}k_{conv}\delta} \|\zeta(t_0)\|. \quad (31)$$

Now, defining the maximum estimation error bound as follows:

$$\zeta_{\max} := \sqrt{\frac{\sigma}{\sigma}} e^{-\frac{\rho}{2}k_{conv}\delta} \|\zeta(t_0)\|. \quad (32)$$

Since the right-hand side of (28) is monotonically decreasing in t , for all $t \geq t_0 + k_{conv}\delta$ it follows that:

$$\|\zeta(t)\| \leq \|\zeta(t_0 + k_{conv}\delta)\| \leq \zeta_{\max}. \quad (33)$$

This proves the existence of a finite bound ζ_{\max} such that

$$\|\zeta(t)\| \leq \zeta_{\max}, \quad \forall t \geq k_{conv}\delta, \quad (34)$$

completing the proof.

5. Main Results

In this section, the main results are presented. The solution to the path-following problem introduced in Section 3 is addressed using a two-stage control strategy as shown in Figure 2. This strategy consists of an outer kinematic guidance loop that provides a reference velocity to an inner surge and yaw rate controller.

5.1. Kinematic Guidance Loop

The objective of the guidance loop is to drive both ϵ and ψ_e to zero. Previous studies employing the VRP approach have often overlooked the influence of the vehicle's attitude ψ in the path-following problem [26, 29]. In most cases, it is only shown that ψ remains bounded due to the system's

internal dynamics [28, 27]. However, in many marine vehicle applications such as docking, station keeping, or visual servoing, large deviations in ψ can lead to mission failure or safety violations

To address this, the error dynamics of ψ_e , defined as $\psi_e = \psi_d - \psi$, are considered. Its time derivative is given by:

$$\dot{\psi}_e = \dot{\psi}_d - r \quad (35)$$

where ψ_d is defined in equation (21). In equation (21), β is an unknown parameter that is estimated as $\hat{\beta}$ using the adaptive observer as in (25).

Equations (35) and (20) together yield the complete error dynamics, expressed as follows:

$$\dot{x}_e = r y_e + U_d \cos(\psi_e) - U \quad (36a)$$

$$\dot{y}_e = -r x_e + U_d \sin(\psi_e) - r E_x \quad (36b)$$

$$\dot{\psi}_e = \dot{\psi}_d - r \quad (36c)$$

At this point, the advantages of the proposed virtual point guidance method are highlighted. In traditional LOS guidance, y_e is minimized by selecting an appropriate heading reference $\psi_d(y_e)$. However, with virtual point guidance, y_e can be directly influenced through r , as it explicitly appears in (36b). Furthermore, ψ_e is also regulated via r , meaning that both errors are minimized using the same virtual input. This coupling necessitates an optimal control approach to balance their simultaneous reduction.

To accomplish this, a NMPC framework is employed. This framework optimally adjusts r while respecting system constraints, offering improved performance. Moreover, the NMPC formulation is integrated with a Controlled Lyapunov Function (CLF) to retain global stability guarantees, following the approach in [36].

Since the sideslip angle β is not directly measurable, the estimation $\hat{\beta}$ by the AEKF is used in the error dynamics, forming the basis for the NMPC problem. Thus, the NMPC optimization relies on the estimated state vector $\hat{\chi}(t_i) \in \mathbb{R}^3$ at time t_i . While not all states need to be estimated, the NMPC uses the available estimates to achieve optimal performance while maintaining constraint adherence.

To formulate the CLF-based NMPC (LNMPC), the error dynamics in equation (36) are rewritten compactly as:

$$\dot{\chi} = f(\chi, u), \quad (37)$$

where $\chi = [x_e, y_e, \psi_e]^T \in \mathbb{R}^3$ is the state vector, and $u = [U, r]^T \in \mathbb{R}^2$ is the virtual control input.

Assumption 6. *The function $f(\chi, u)$ is assumed to be locally Lipschitz continuous in both χ and u on a domain containing the origin. Specifically, there exists a constant $L > 0$ such that for all $\chi_1, \chi_2 \in \mathbb{R}^3$ and $u_1, u_2 \in \mathbb{R}^2$:*

$$\|f(\chi_1, u_1) - f(\chi_2, u_2)\| \leq L \|\chi_1 - \chi_2\| \quad (38)$$

where L is the Lipschitz constant associated with $f(\chi, u)$. The origin is an equilibrium point for the nominal system, i.e., $f(0, 0) = 0$.

Given the error system (37) and the adaptive observer (25), the open-loop optimization problem at each time instant t_i ($i \geq 0$) is formulated as:

$$\min_{\bar{u}(\cdot)} J(\hat{\chi}(t_i), \bar{u}(\cdot)) = \int_{t_i}^{t_i+T_p} \left(\|\bar{\chi}(t_i, \tau)\|_Q^2 + \|\bar{u}(t_i, \tau)\|_R^2 \right) d\tau \quad (39a)$$

subject to:

$$\dot{\bar{\chi}}(\tau) = f(\bar{\chi}(t_i, \tau), \bar{u}(t_i, \tau)), \quad (39b)$$

$$\bar{\chi}(t_i) = \hat{\chi}(t_i) \quad (39c)$$

$$\bar{u}(\tau) \in \mathcal{U}, \quad (39d)$$

$$\frac{\partial V_1}{\partial \chi} f(\bar{\chi}(t_i, \tau), \bar{u}(\hat{\chi}(t_i), \tau)) \leq \frac{\partial V_1}{\partial \chi} f(\bar{\chi}(t_i, \tau), \bar{u}(\hat{\chi}(t_i), \tau)) \quad (39e)$$

The objective is to minimize the cost function J , which includes a weighted sum of the state error and control effort over the prediction horizon T_p . The function $f(\bar{\chi}, \bar{u})$ describes the system dynamics, while $\bar{\chi}(t_i, \tau)$ and $\bar{u}(t_i, \tau)$ denote predicted state and input trajectories. The matrices Q , R , and P are positive definite weights penalizing state deviation, control effort, and terminal error, respectively. The control constraint set is defined as $\mathcal{U} = \{u \in \mathbb{R}^2 \mid u_{\min} \leq u_i \leq u_{\max}\}$ for $i = 1, 2$. Here, $V_1(\cdot)$ is the CLF, and \bar{u} is the auxiliary controller ensuring satisfaction of the constraint (39e), presented in the later part of this section.

At each sampling instant, the LNMPC solves the optimization problem to determine the optimal control sequence. Based on the observer-estimated state $\hat{\chi}$, the system's future behavior is predicted using $f(\bar{\chi}, \bar{u})$. After solving the optimization problem, only the first control input $\bar{u}^*(\cdot, \hat{\chi}(t_i))$ is applied. This receding horizon approach enhances robustness against model uncertainty and external disturbances.

Auxiliary Lyapunov based controller

To design the auxiliary controller introduced in the LNMPC problem is addressed here. Let the Lyapunov function be defined as:

$$V_1(\chi) = \frac{1}{2}(x_e^2 + y_e^2) \quad (40)$$

Taking the time derivative of V_1 along the system dynamics yields:

$$\dot{V}_1 = x_e \dot{x}_e + y_e \dot{y}_e \quad (41)$$

Substituting the system dynamics, we obtain:

$$\begin{aligned} \dot{V}_1 &= x_e(\dot{\psi} y_e + U_d \cos(\psi_e) - U) \\ &\quad + y_e(-\dot{\psi} x_e + U_d \sin(\psi_e) - r E_x) \end{aligned} \quad (42)$$

Now by choosing the feedback control law $\tilde{u} = [U, r]^T$ given as:

$$U = U_d \cos \psi_e + k_1 x_e \quad (43a)$$

$$r = \frac{U_d \sin \psi_e + k_2 y_e}{E_x} \quad (43b)$$

Finally, substituting the control law (43) in \dot{V}_1 we obtain:

$$\begin{aligned} \dot{V}_1 &= -k_1 x_e^2 - k_2 y_e^2 \\ &= -\alpha V_1 \end{aligned} \quad (44)$$

where α is $\min(\frac{k_1}{2}, \frac{k_2}{2})$. Thus, if $k_1 > 0$ and $k_2 > 0$ any states $\chi \in \mathcal{W}$ (will be defined later), the system states remain bounded and asymptotically converge to equilibrium.

Note that ψ_e is not included in the Lyapunov function. This is because orientation error ψ_e remains bounded under the proposed control law, even though it is not directly included in the Lyapunov function. From the closed-loop dynamics, we have

$$\dot{\psi}_e = \dot{\psi}_d - r = \dot{\psi}_d - \frac{U_d \sin \psi_e + k_2 y_e}{E_x} \quad (45)$$

where $\dot{\psi}_d$ is the desired angular rate and it is bound such that there exists a $|\dot{\psi}_d| \leq \dot{\psi}_d^{\max}$. Define the auxiliary function $V_2 = 1 - \cos \psi_e$, which is positive definite and radially unbounded with respect to ψ_e . Taking the time derivative yields

$$\dot{V}_2 = \sin \psi_e \cdot \dot{\psi}_e = \sin \psi_e \left(\dot{\psi}_d - \frac{U_d \sin \psi_e + k_2 y_e}{E_x} \right) \quad (46)$$

This simplifies to

$$\dot{V}_2 = \dot{\psi}_d \sin \psi_e - \frac{U_d}{E_x} \sin^2 \psi_e - \frac{k_2}{E_x} y_e \sin \psi_e. \quad (47)$$

Since $\dot{\psi}_d$ is bounded and $y_e(t) \rightarrow 0$ as $t \rightarrow \infty$, the last term vanishes asymptotically. For sufficiently large t , \dot{V}_2 is bounded by

$$\dot{V}_2 \leq \dot{\psi}_d^{\max} |\sin \psi_e| - \frac{U_d}{E_x} \sin^2 \psi_e \quad (48)$$

This expression defines a concave quadratic in $|\sin \psi_e|$ with a maximum, implying that for large enough ψ_e , the dissipative term dominates, and $\dot{V}_2 < 0$. Thus, $V_2(t)$ cannot increase indefinitely, and $\psi_e(t)$ must remain bounded. Therefore, under the proposed control law, the heading error ψ_e remains bounded for all time.

Now the level set, where the system is expected to converge, is chosen as:

$$\mathcal{W}_C = \{(x_e, y_e, \psi_e) \mid V_1(\chi) \leq C\} \quad (49)$$

If the proposed controllers (43) satisfy the input constraints \mathcal{U} , then the upper bound on δ is given by:

$$C \leq \min \left(\frac{(U_{\max} - U_d \cos(\psi_e))^2}{2k_1^2}, \frac{(r_{\max} E_x - U_d \sin \psi_e)^2}{2k_2^2} \right) \quad (50)$$

The choice of the level set \mathcal{W} is crucial because it ensures recursive feasibility, provided disturbances remain within allowable bounds.

Stability of the LNMPC

The stability of the closed-loop LNMPC combined with an AEKF observer is based on the existence of a continuous value function that remains inherently robust to the state estimation error introduced by the AEKF. This estimation error acts as a disturbance in the closed-loop system but does not destabilize it as proven in the following theorem.

Theorem 2. Consider the error dynamics (37) subject to the LNMPC scheme defined in (39), where the estimated state $\hat{\chi}(t)$ is provided by an AEKF. Suppose the following conditions hold:

- The true system dynamics satisfy the Lipschitz continuity condition stated in Assumption 6.
- There exists a control Lyapunov function $V_1(\chi)$ satisfying the CLF condition (39e) under the auxiliary control law (43), within the set $\mathcal{W}_C = \{(x_e, y_e, \psi_e) \mid V_1(\chi) \leq C\}$.
- The observer satisfies the bounded estimation error condition $\|\chi(t_i) - \hat{\chi}(t_i)\| \leq \zeta_{\max}$ for all $t_i \geq K_{\text{conv}}\delta$, where K_{conv} denotes the observer convergence time.

Then, for all sampling times $\delta \leq \delta_{\max}$ and estimation error bounds $\zeta \leq \zeta_{\max}$ satisfying the bounds (52) and (60), the following properties hold:

1. (**Recursive Feasibility**) The LNMPC optimization problem remains feasible at all sampling instants t_i .
2. (**Convergence**) For any initial condition $\chi(0) \in \mathcal{W}_{C_0} \subset \mathcal{W}_C$, the closed-loop trajectory $\chi(t)$ converges to the set $\mathcal{W}_{\alpha/2} \subset \mathcal{W}_\alpha \subset \mathcal{W}_C$, and remains within \mathcal{W}_α thereafter.

PROOF. Step 1: Recursive Feasibility: Consider any sampling instant t_i at which a feasible solution exists i.e., $(\bar{u}^*(\cdot, \chi(t_i)))$, meaning the LNMPC problem has an optimal solution that ensures both constraint satisfaction and proper system dynamics evolution.

Between t_i and t_{i+1} , the control input applied to the system is $\bar{u}^*(\cdot, \chi(t_i))$. The remainder of the optimal input sequence, $\bar{u}^*(\tau, \chi(t_i))$, for $\tau \in [t_{i+1}, t_i + T_p]$, continues to satisfy the system constraints. Furthermore, for all $\chi(t_i +$

$T_p) \in \mathcal{W}_C$, there exists an auxiliary control law $\bar{u}(\cdot)$ such that, the CLF condition (39e) and the control constraint (39d) are satisfied. For any time $t_i + \sigma$, where $\sigma \in (0, t_{i+1} - t_i]$, the control input is defined as:

$$\bar{u}(\tau, \chi(t_i + \sigma)) = \begin{cases} \bar{u}^*(\tau, \hat{\chi}(t_i)), & \text{for } \tau \in [t_{i+1}, t_i + T_p], \\ \bar{u}(\tau - t_i - T_p), & \text{for } \tau \in (t_i + T_p, t_i + T_p + \sigma]. \end{cases} \quad (51)$$

Since $\bar{u}(\cdot, \chi(t_{i+1}))$ satisfies all state and input constraints and preserves the CLF condition due to the terminal auxiliary control law \bar{u} , recursive feasibility of the LNMPC optimization problem at time t_{i+1} is guaranteed.

Step 2: Convergence The convergence is proven in two parts.

Part one: For any initial state $\chi(0) \in \mathcal{W}_{C_0}$, which is strictly contained within \mathcal{W}_C , the state will reach a set \mathcal{W}_{C_1} where $C_1 = C_0 + (C - C_0)/2$ after some $T_{C_0C_1}$. The existence of such a $T_{C_0C_1}$ is guaranteed under the assumption (6), because $\forall \chi(\tau) \in \mathcal{W}_C$ then, we have $\|\chi(\tau) - \chi(0)\| \leq \int_0^\tau \|f(\chi(t), u(t))\| dt \leq K_{\mathcal{W}_C} t$ where the $K_{\mathcal{W}_C}$ is a constant depending on the Lipschitz constant of $f(\chi, u)$ and the bound on u . Let $T_{C_0C_1}$ be the minimum time required to reach the boundary of \mathcal{W}_{C_1} , from any point $\chi(0) \in \mathcal{W}_{C_0}$ allowing $u(t)$ to take admissible values in \mathcal{U} . By similar arguments, there also exists a time T_{C_2C} such that for all $\chi(t_i) \in \mathcal{W}_{C_2}$, the state $\chi(\tau) \in \mathcal{W}_C$ for all $\tau \in [t_i, t_i + T_{C_2C}]$. where $C_2 = C_1 + (C - C_1)/2$. We now pick the maximum sampling time δ_{\max} as

$$\delta_{\max} = \min \left\{ T_{C_0C_1}/k_{\text{Conv}}, T_{C_2C} \right\} \quad (52)$$

Thus, any initial state in \mathcal{W}_{C_0} does not leave the level set \mathcal{W}_C during the convergence of observer $K_{\text{conv}}\delta_{\max}$.

part two: Since the Lyapunov function $V_1(\chi)$ is continuously differentiable and radially unbounded, we can apply converse Lyapunov theorems there exists a functions β_1 , β_2 and β_3 that belongs to \mathcal{K}_∞ such that the following inequalities hold:

$$\beta_1(\|\chi\|) \leq V_1(\chi) \leq \beta_2(\|\chi\|) \quad (53a)$$

$$\frac{\partial V_1}{\partial \chi} f(\chi, \bar{u}) \leq -\beta_3(\|\chi\|) \quad (53b)$$

Furthermore from the (39e) and (39d) we have the following inequality:

$$\begin{aligned} \frac{\partial V_1}{\partial \chi} f(\bar{\chi}(t_i, \tau), \bar{u}^*(\hat{\chi}(t_i), \tau)) &\leq \frac{\partial V_1}{\partial \chi} f(\bar{\chi}(t_i, \tau), \bar{u}(\hat{\chi}(t_i), \tau)) \\ &\leq -\beta_3(\|\chi\|) \end{aligned} \quad (54)$$

Now, for any $\chi(t_i) \in \mathcal{W}_{C_1}$, the time derivative of the Lyapunov function along the trajectory state trajectory $\chi(\tau)$ of the system, $\forall \tau \in [t_i, t_i + 1)$

$$\dot{V}_1(\chi(\tau)) = \frac{\partial V_1}{\partial \chi} f(\chi(\tau), \bar{u}^*(\hat{\chi}(t_i), \tau)) \quad (55)$$

By adding and subtracting the term $\frac{\partial V_1}{\partial \chi} f(\bar{\chi}(t_i, \tau), -\bar{u}^*(\hat{\chi}(t_i), \tau))$ and taking (54) into consideration, one gets:

$$\begin{aligned} \dot{V}_1(\chi(\tau)) &= \frac{\partial V_1}{\partial \chi} f(\chi(\tau), \bar{u}^*(\hat{\chi}(t_i), \tau)) \\ &+ \frac{\partial V_1}{\partial \chi} f(\bar{\chi}(t_i, \tau), \bar{u}^*(\hat{\chi}(t_i), \tau)) \\ &- \frac{\partial V_1}{\partial \chi} f(\bar{\chi}(t_i, \tau), \bar{u}^*(\hat{\chi}(t_i), \tau)) \quad (56) \\ &= -\beta_3(\|\chi\|) + \frac{\partial V_1}{\partial \chi} f(\chi(\tau), \bar{u}^*(\hat{\chi}(t_i), \tau)) \\ &- \frac{\partial V_1}{\partial \chi} f(\bar{\chi}(t_i, \tau), \bar{u}^*(\hat{\chi}(t_i), \tau)) \end{aligned}$$

Since function $f(\chi, u)$ is Lipschitz continuous (Assumption 6) and V_1 is continuously differentiable, then $\frac{\partial V_1}{\partial x} f(\cdot)$ is also Lipschitz. Thus we have:

$$\dot{V}_1(\chi(\tau)) = -\beta_3(\|\chi\|) + L_V \|\chi(\tau) - \bar{\chi}(t_i, \tau)\| \quad (57)$$

here, L_V is the Lipschitz constant associated with $\frac{\partial V_1}{\partial \chi} f(\chi, u)$.

The prediction error between $\chi(\tau)$ and $\bar{\chi}(t_i, \tau)$ is related to the state estimation error and it can be bounded using the Grönwall-Bellman inequality as follows:

$$\|\chi(\tau) - \bar{\chi}(t_i, \tau)\| \leq e^{L_f \tau} \|\chi(t_i) - \hat{\chi}(t_i)\| \quad (58)$$

where L_f is the Lipschitz constant associated with $f(\cdot)$. We thus obtain the bound on $\dot{V}_1(\chi(\tau))$:

$$\dot{V}_1(\chi(\tau)) = -\beta_3(\|\chi\|) + L_V e^{L_f \tau} \|\chi(t_i) - \hat{\chi}(t_i)\| \quad (59)$$

Now assuming that $x(\tau) \notin \mathcal{W}_{\alpha/2}$ i.e., $\|\chi\| \geq \alpha/2$ and since $\beta_3 \in K_\infty$, we have $\beta_3(\|\chi\|) \geq \beta_3(\alpha/2)$. Hence for any χ to converge to the set $\mathcal{W}_{\alpha/2}$, From Theorem 1, there exists a bound $|\chi(t_i) - \hat{\chi}(t_i)| \leq \zeta_{\max}$, and the observer parameter ζ_{\max} should be chosen such that:

$$L_V(e^{L_f \tau} \zeta_{\max}) \leq \beta_3(\alpha/2) \quad (60)$$

where e_{\max} the maximum estimation error after the convergence time $K_{conv} \delta$.

Integrating both sides over the interval $[t_i, t_i + 1]$, we get:

$$V_1(\chi(t_i + 1)) - V_1(\chi(t_i)) \leq -\beta_3(\alpha/2) \quad (61)$$

which implies:

$$V_1(\chi(t_i + 1)) \leq V_1(\chi(t_i)) - \beta_3(\alpha/2) \quad (62)$$

By recursively applying the inequality, we conclude that if any $\chi(0) \in \mathcal{W}_{C_0}$ will converge to $\mathcal{W}_{\alpha/2}$ in a finite time without leaving the admissible set \mathcal{W}_C if the observer parameters satisfies (52) and (60). Once the system reaches $\mathcal{W}_{\alpha/2}$, it will remain inside \mathcal{W}_α . this statement holds because the $\mathcal{W}_{\alpha/2} \subseteq \mathcal{W}_\alpha$.

5.2. Kinetic Control Loop

At the kinetics level, the virtual desired velocities generated by the guidance stage are tracked by designing the input thrusts. To achieve this, we employ a neural adaptive sliding mode control strategy as proposed in [37]. We define the tracking errors as $u_e = u - u_r$ and $r_e = r - r_r$, and introduce the following sliding surfaces:

$$s_{u_e} = u_e + \lambda_{u_e} \int u_e dt \quad (63a)$$

$$s_{r_e} = r_e + \lambda_{r_e} \int r_e dt \quad (63b)$$

where $\lambda_{(\cdot)}$ are positive design constants. The time derivatives of the sliding surfaces are given by:

$$\begin{aligned} \dot{s}_{u_e} &= \dot{u}_e + \lambda_{u_e} u_e \\ &= f_u(u, v, r) + \Delta_{f_u} + \tau_u + d_u - \dot{u}_r + \lambda_{u_e} u_e \quad (64a) \end{aligned}$$

$$\begin{aligned} \dot{s}_{r_e} &= \dot{r}_e + \lambda_{r_e} r_e \\ &= f_r(u, v, r) + \Delta_{f_r} + \tau_r + d_r - \dot{r}_r + \lambda_{r_e} r_e \quad (64b) \end{aligned}$$

where $\Delta_{(\cdot)}$ represent model uncertainties and unmodeled dynamics. These uncertainties are approximated using Radial Basis Function Neural Networks (RBF-NNs) as $\hat{\Delta}_{(\cdot)} = \hat{W}_{(\cdot)} \mu_{(\cdot)}$, where $\hat{W}_{(\cdot)}$ are the estimated neural network weights, and $\mu_{(\cdot)}$ are Gaussian basis functions. The weight estimation error is denoted by $\tilde{W}_{(\cdot)} = \hat{W}_{(\cdot)} - W_{(\cdot)}^*$, where W^* are the ideal weights.

To enforce convergence, the sliding surface dynamics are designed to follow the following reaching law:

$$\dot{s}_{u_e} = -k_{u_e} s_{u_e} - D_{u_e} \text{sign}(s_{u_e}) \quad (65a)$$

$$\dot{s}_{r_e} = -k_{r_e} s_{r_e} - D_{r_e} \text{sign}(s_{r_e}) \quad (65b)$$

where $k_{(\cdot)}$ are positive gains and $D_{(\cdot)}$ are disturbance compensation terms. These are estimated adaptively to account for external disturbances $d_{(\cdot)}$ and approximation errors of the neural network. Let $\hat{D}_{(\cdot)}$ denote the estimates of these terms, and $\tilde{D}_{(\cdot)} = \hat{D}_{(\cdot)} - d_{(\cdot)}$ their estimation errors.

By combining (64) and (65), the control inputs τ_u and τ_r are designed to enforce the reaching law as follows:

$$\tau_u = -f_u(u, v, r) - \hat{\Delta}_{f_u} + \dot{u}_r - \lambda_{u_e} u_e - k_{u_e} s_{u_e} - \hat{D}_{u_e} \text{sign}(s_{u_e}) \quad (66a)$$

$$\tau_r = -f_r(u, v, r) - \hat{\Delta}_{f_r} + \dot{r}_r - \lambda_{r_e} r_e - k_{r_e} s_{r_e} - \hat{D}_{r_e} \text{sign}(s_{r_e}) \quad (66b)$$

Stability of the Control Loop

To analyze the stability of the proposed adaptive sliding mode controller, we define a Lyapunov function candidate as:

$$\begin{aligned} V &= \frac{1}{2} s_{u_e}^2 + \frac{1}{2} s_{r_e}^2 + \frac{1}{2} \text{tr}(\tilde{W}_u^T \Gamma_u^{-1} \tilde{W}_u) + \frac{1}{2} \text{tr}(\tilde{W}_r^T \Gamma_r^{-1} \tilde{W}_r) \\ &+ \frac{1}{2} \tilde{D}_{u_e}^2 + \frac{1}{2} \tilde{D}_{r_e}^2 \quad (67) \end{aligned}$$

$\Gamma_{(\cdot)}$ are positive-definite learning rate matrices.

Taking the time derivative of V yields:

$$\begin{aligned} \dot{V} = & s_{u_e} \dot{s}_{u_e} + s_{r_e} \dot{s}_{r_e} + \text{tr} \left(\tilde{W}_u^T \Gamma_u^{-1} \dot{\tilde{W}}_u \right) + \text{tr} \left(\tilde{W}_r^T \Gamma_r^{-1} \dot{\tilde{W}}_r \right) \\ & + \tilde{D}_{u_e} \dot{\tilde{D}}_{u_e} + \tilde{D}_{r_e} \dot{\tilde{D}}_{r_e} \end{aligned} \quad (68)$$

Using the error dynamics and control laws from Eq. (64) and Eq. (65), we substitute:

$$\dot{s}_{u_e} = -k_{u_e} s_{u_e} - D_{u_e} \text{sign}(s_{u_e}) + \tilde{\Delta}_{f_u} + \tilde{D}_{u_e} \text{sign}(s_{u_e}) \quad (69)$$

$$\dot{s}_{r_e} = -k_{r_e} s_{r_e} - D_{r_e} \text{sign}(s_{r_e}) + \tilde{\Delta}_{f_r} + \tilde{D}_{r_e} \text{sign}(s_{r_e}) \quad (70)$$

Substituting these into \dot{V} :

$$\begin{aligned} \dot{V} = & -k_{u_e} s_{u_e}^2 - k_{r_e} s_{r_e}^2 + s_{u_e} \tilde{\Delta}_{f_u} + s_{r_e} \tilde{\Delta}_{f_r} + \tilde{D}_{u_e} |s_{u_e}| \\ & + \tilde{D}_{r_e} |s_{r_e}| + \text{tr} \left(\tilde{W}_u^T \Gamma_u^{-1} \dot{\tilde{W}}_u \right) + \text{tr} \left(\tilde{W}_r^T \Gamma_r^{-1} \dot{\tilde{W}}_r \right) \\ & + \tilde{D}_{u_e} \dot{\tilde{D}}_{u_e} + \tilde{D}_{r_e} \dot{\tilde{D}}_{r_e} \end{aligned} \quad (71)$$

To cancel the NN approximation and disturbance terms, we define the adaptive update laws:

$$\dot{\tilde{W}}_u = \Gamma_u s_{u_e} \mu_u \quad (72a)$$

$$\dot{\tilde{W}}_r = \Gamma_r s_{r_e} \mu_r \quad (72b)$$

$$\dot{\tilde{D}}_{u_e} = \gamma_{D_u} |s_{u_e}| \quad (72c)$$

$$\dot{\tilde{D}}_{r_e} = \gamma_{D_r} |s_{r_e}| \quad (72d)$$

Substituting these into the Lyapunov derivative leads to:

$$\dot{V} = -k_{u_e} s_{u_e}^2 - k_{r_e} s_{r_e}^2 \leq 0 \quad (73)$$

Since $\dot{V} \leq 0$, the Lyapunov function is non-increasing and bounded below. Thus, sliding surface is asymptotically stable, i.e.,

$$\lim_{t \rightarrow \infty} s_{u_e}(t) = 0, \quad \lim_{t \rightarrow \infty} s_{r_e}(t) = 0 \quad (74)$$

Because of (63), we also have:

$$\lim_{t \rightarrow \infty} u_e(t) = 0, \quad \lim_{t \rightarrow \infty} r_e(t) = 0 \quad (75)$$

Therefore, the proposed controller guarantees that all signals remain bounded, and the tracking errors asymptotically converge to zero in the presence of modeling uncertainty and bounded external disturbances.

Remark 6. Note that the sway dynamics (v), are not explicitly included in the stability analysis. However, it can be shown that v remains uniformly bounded for any $Y_1, Y_2 \geq 0$ in (4b), provided that the surge velocity u , yaw rate r , and disturbance d_v are bounded, as demonstrated in [38]. Moreover, most AMVs are designed such that the conditions $Y_1, Y_2 \geq 0$ are naturally satisfied (see Remark 3 in [28]).

Remark 7. The overall stability of the closed-loop system, comprising both the guidance loop and the kinetic control loop discussed above, can be analyzed using singular perturbation theory (See [39], Chapter. 11). In this framework, the control loop operates on a faster timescale compared to the guidance loop, owing to the relative separation in their dynamic responses. By treating the guidance system as a slow subsystem and the control dynamics as a fast subsystem, one can demonstrate that the composite system remains stable under the Tikhonov theorem conditions (See [39], Chapter. 11, Section 2). This entails proving that both the reduced slow system and the boundary-layer fast system are stable in isolation and that the fast subsystem converges quickly to a quasi-steady state. However, for brevity, this detailed analysis is omitted here as the primary focus of this work is on the VRP-based guidance strategy.

6. Case study: Blucy

Blucy is an underactuated underwater vehicle used for non-invasive underwater monitoring. The vehicle is equipped with six thrusters, as shown in Fig. 3: two longitudinal thrusters for surge, two lateral thrusters for yaw control, and two vertical thrusters for depth and heave control without inducing pitch.

The pitch and roll dynamics are inherently stable due to hydrostatic restoring forces resulting from the vertical offset between the center of gravity (CoG) and the center of buoyancy (CoB). This design satisfies all assumptions outlined in Section 2 for the 3-DOF planar motion model. The physical parameters of the vehicle were experimentally identified and validated by the authors in [40].



Figure 3: Blucy underwater vehicle with 6-thruster configuration.

6.1. Simulation Results

The proposed guidance and control framework is implemented and tested in a MATLAB/Simulink environment. The LNMPC guidance scheme is compared against the method proposed in [26] in two scenarios: (i) straight-line path following, and (ii) curved path following — both in the presence of external disturbances.

Parameter Settings: The observer and controller parameters used in simulation are as follows: - The adaptive observer parameters: $\rho_z = 5$, $\rho_\beta = 0.2$ and $\Sigma = 1.5I_{2 \times 2}$. The LNMPC parameters: The sampling period $\delta = 0.1$, the prediction horizon is $T_p = 5$. The weight matrices $Q = \text{diag}(5, 5, 2)$, and $R = \text{diag}(3, 3)$ and the limit on the $U = [0, 1]m/sec$ and $r = [-0.01, 0.01]rad/sec$, the auxiliary control gain $k_1 = 0.8$ and $k_2 = 1$. The control loop parameters: $\lambda_{u_e} = 0.1$, $\lambda_{r_e} = 0.2$, $\gamma_{D_u} = 3$, $\gamma_{D_r} = 5$, $\Gamma_u = 10$ and $\Gamma_r = 10$. The virtual reference point $E_x = 0.8m$ and $E_y = 0$.

(i) **Straight-Line Path:** In this scenario, the vehicle is tasked with following a straight-line path at a constant depth of 5 m, defined parametrically as:

$$\begin{aligned} x(\zeta) &= x_0 + \zeta, \\ y(\zeta) &= y_0 + 0.5\zeta, \end{aligned}$$

where ζ is the arc-length parameter along the path, and the slope of the trajectory in the (x, y) -plane is 0.5. This corresponds to a desired heading angle ψ of approximately 26.6 deg.

The initial conditions for the vehicle are set as: $x_0 = 0$ m, $y_0 = 5$ m, $\psi_0 = 0$ deg, $u_0 = 0$ m/s, $v_0 = 0$ m/s, and $r_0 = 0$ deg/s. The total simulation time is 150 seconds.

To evaluate the robustness of the guidance scheme, an external wind disturbance is introduced. It is modeled as a constant velocity field with wind speed of 0.1 m/s, flowing from 180° (i.e., southward) in the inertial reference frame.

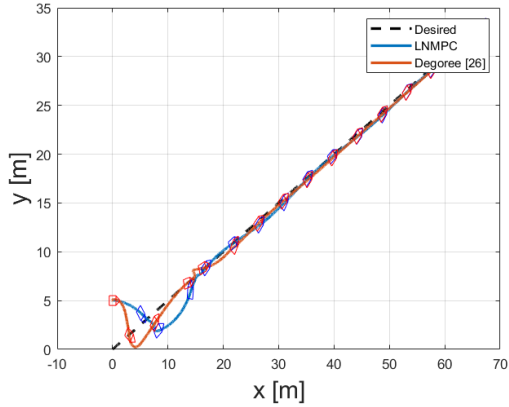


Figure 4: Trajectory comparison for straight-line path following under wind disturbance.

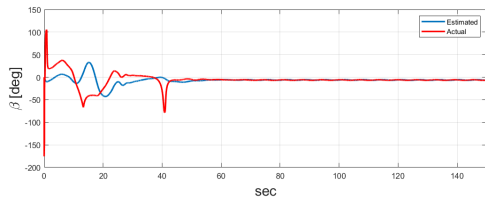
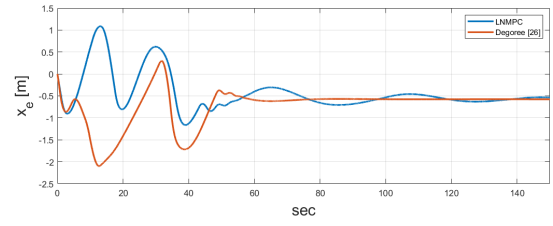
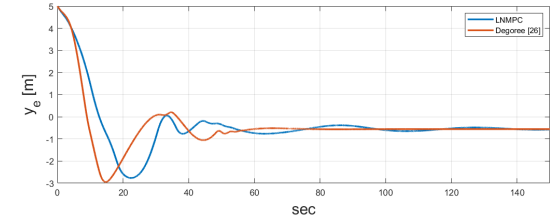


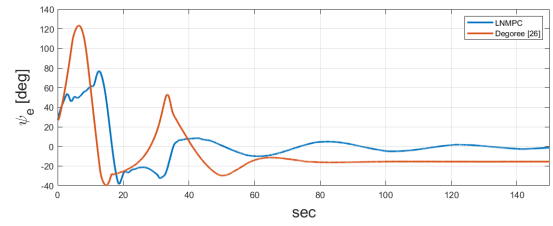
Figure 5: Sideslip angle β estimated using the AEKF observer.



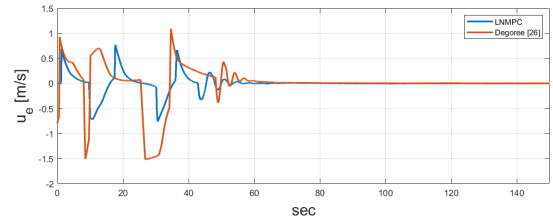
(a) Position error: x_e .



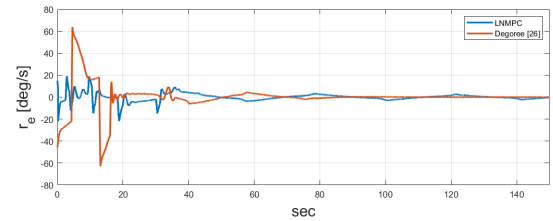
(b) Position error: y_e .



(c) Heading angle error: ψ_e .



(d) Surge velocity error: u_e .



(e) Yaw rate error: r_e .

Figure 6: Tracking performance comparison : Position (X_e , Y_e), heading angle (ψ_e), and velocity errors (u_e , r_e) between the proposed LNMPC and the method in [26].

The simulation results for the straight-line path-following scenario underscore the effectiveness of the proposed LNMPC approach, particularly in enhancing attitude regulation while maintaining comparable position tracking performance. As shown in Figure 4, both the LNMPC and the reference controller from [26] successfully follow the desired trajectory despite the presence of steady wind disturbances.

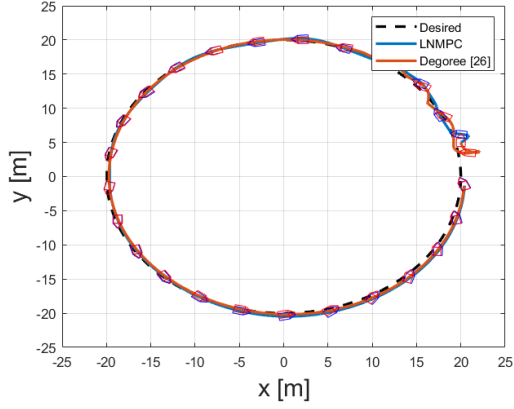


Figure 7: Trajectory comparison for curved path following under wind disturbances.

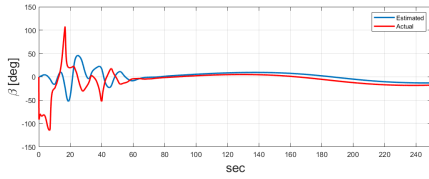


Figure 8: Sideslip angle β estimated using the AEKF observer.

However, the LNMPC demonstrates reduced lateral deviation during transients and achieves smoother convergence to the desired path.

Figure 5 presents the estimation of the sideslip angle β using the AEKF observer, which provides critical feedback for attitude control. Accurate real-time estimation of β enhances the heading feedback and contributes to the performance of the LNMPC in attitude regulation.

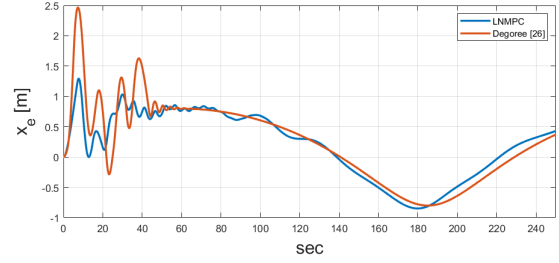
The LNMPC achieves faster alignment with the desired heading and maintains more stable behavior compared to the baseline controller. This improvement is supported by the heading error ψ_e in Figure 6c, where the LNMPC significantly reduces steady state error and oscillations, resulting in a more reliable heading response.

In contrast, the position errors X_e and Y_e (Figures 6a,6b) as well as velocities errors u_e and r_e (Figures 6d,6e) are similar in magnitude between the two controllers. Nonetheless, the LNMPC displays smoother error transients and better damping characteristics, indicative of improved closed-loop behavior.

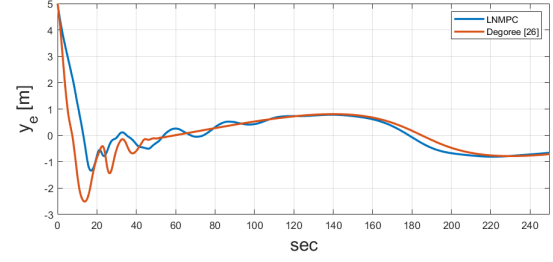
(ii) *Curved Path:* In this scenario, the vehicle is commanded to follow a curved trajectory defined by a circular arc in the horizontal plane. The path is described parametrically as:

$$\begin{aligned} x(\zeta) &= R \cos(\zeta), \\ y(\zeta) &= R \sin(\zeta), \end{aligned}$$

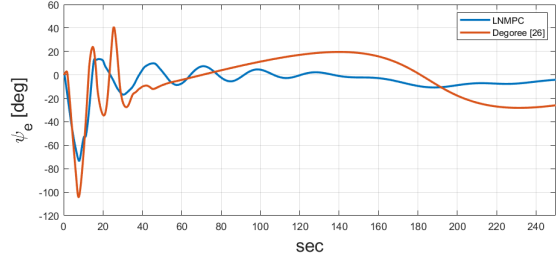
where $R = 20$ m is the radius of the circular path and ζ is the path parameter representing angular progression along the arc. The vehicle is initialized at position $(x_0, y_0) =$



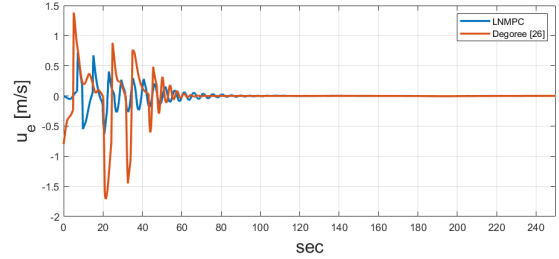
(a) Position error: x_e .



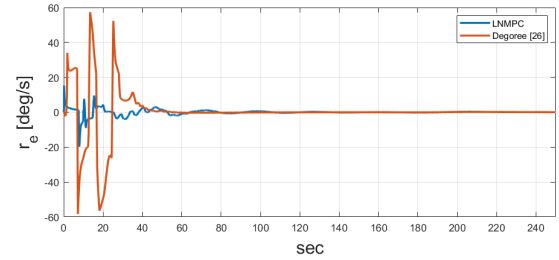
(b) Position error: y_e .



(c) Heading angle error: ψ_e .



(d) Surge velocity error: u_e .



(e) Yaw rate error: r_e .

Figure 9: Tracking performance comparison: Position (X_e , Y_e), heading angle (ψ_e), and velocity errors (u_e , r_e) between the proposed LNMPC and the method in [26].

(20 m, 5 m) with an initial heading $\psi_0 = 90^\circ$, and with zero

Path	Term	LN MPC	[26]	Improvement (%)
Straight Line	Position	171.4	176.4	2.84%
	Heading	30.16	58.4	48.34%
Curved	Position	227	241	5.81%
	Heading	33.29	73.7	54.83%

Table 1

Quantitative analysis of tracking error comparison between the proposed LN MPC method and the approach in [26] using integrated absolute errors. The improvement column indicates the percentage reduction in error achieved by LN MPC relative to the reference method, where lower values signify better tracking performance.

surge velocity and yaw rate: $u_0 = 0$ m/s, $r_0 = 0$ rad/s. The total simulation duration is 250 seconds.

As in the straight-line case, a steady wind disturbance of 0.1 m/s from 180° (southward direction in the inertial frame) is applied to evaluate the robustness of the controller under environmental influences. This scenario challenges both the position tracking and the vehicle's ability to continuously adapt its heading as the curvature of the path evolves. The goal is to test the controller's capability to maintain precise attitude regulation while following a dynamically changing reference orientation.

Figure 7 shows the trajectory tracking performance under this curved path scenario. Both controllers are able to follow the desired circular path, but the proposed LN MPC demonstrates faster convergence and reduced initial path deviation, especially near regions of higher curvature. The trajectory produced by the LN MPC is smoother and less oscillatory in response to wind disturbance, confirming the robustness of the approach.

The heading dynamics are further analyzed in Figure 8, which presents the sideslip angle β estimated using the AEKF observer. The LN MPC maintains more stable and bounded β dynamics compared to the controlled method in [26], reflecting improved estimation consistency and better adaptation to environmental effects.

Figure 9 details the error dynamics. While both methods eventually settle to similar steady-state tracking accuracy for position errors (x_e , y_e), the LN MPC shows smoother transient responses. Most notably, Figure 9c highlights a substantial improvement in heading error ψ_e , where the proposed controller maintains faster convergence, smaller amplitude oscillations and lower steady state error. In terms of velocities (Figures 9d, 9e), LN MPC provides better damping in the transient regime while maintaining comparable steady-state behavior to the controller proposed in [26].

These results are further supported by the quantitative analysis using time-integrated absolute errors presented in Table 1. The most significant improvements are observed in heading control, with error reductions of 48.34% and 54.83% for the straight and curved paths, respectively. While position errors also decreased—by 2.84% and 5.81%—the

performance gains in this case are more modest. These findings highlight the effectiveness of the LN MPC in enhancing heading tracking accuracy, particularly in complex path-following scenarios.

7. Conclusion

This paper presented a VRP guidance strategy as an alternative to traditional LOS guidance for a class of AMVs. Unlike conventional VRP-based methods, which typically do not explicitly account for attitude dynamics, this work attempts to control the neglected attitude regulation in the presence of ocean currents and environmental disturbances. We show that by explicitly addressing the heading dynamics within the control design, more accurate and robust path following can be achieved.

To address this challenge, we formulated the tracking error dynamics in the body-fixed reference frame and demonstrated that both cross-track and heading errors can be simultaneously regulated via yaw rate control. Accordingly, we proposed a LN MPC that optimally minimizes position and heading errors. This controller is augmented by an AEKF observer that estimates the sideslip angle β , a quantity for accurate attitude representation in the presence ocean currents and disturbances.

By incorporating β into the prediction model, the LN MPC achieves improved heading accuracy and robustness to external disturbances, as demonstrated through high-fidelity simulation results. The proposed method shows superior performance in attitude regulation compared to the control strategy from [26], while maintaining comparable position tracking accuracy.

Future work will focus on experimental validation of the controller on a physical marine vehicle and extending the framework to accommodate more advanced scenarios, such as obstacle avoidance and time-varying path planning. Additionally, the proposed methodology can be adapted to vehicles with vertical control (e.g., using pitch to regulate depth), where attitude control becomes even more critical. As discussed in [26], VRP-based guidance has the potential to address underactuation via kinematic coupling, but it may lead to undesirable attitude configurations (e.g., inverted tracking). The proposed approach offers a robust solution to such issues and enables VRP guidance to be effectively applied to reconfigurable and more complex marine vehicles.

Declaration of Generative AI and AI-assisted Technologies in the Writing Process

During the preparation of this work, the author(s) used ChatGPT by OpenAI to assist with language editing, improving clarity, and refining the structure of technical content. After using this tool, the author(s) reviewed and edited the content as necessary and take(s) full responsibility for the final version of the manuscript.

References

- [1] C. Whitt, J. Pearlman, B. Polagye, F. Caimi, F. Muller-Karger, A. Coping, H. Spence, S. Madhusudhana, W. Kirkwood, L. Grosjean, et al., Future vision for autonomous ocean observations, *Frontiers in Marine Science* 7 (2020) 697.
- [2] F. Di Ciaccio, S. Troisi, Monitoring marine environments with autonomous underwater vehicles: A bibliometric analysis, *Results in Engineering* 9 (2021) 100205.
- [3] F. Nauert, P. Kampmann, Inspection and maintenance of industrial infrastructure with autonomous underwater robots, *Frontiers in Robotics and AI* 10 (2023) 1240276.
- [4] H. Mansor, M. H. Norhisam, Z. Z. Abidin, T. S. Gunawan, Autonomous surface vessel for search and rescue operation, *Bulletin of Electrical Engineering and Informatics* 10 (2021) 1701–1708.
- [5] A. Boretti, Unmanned surface vehicles for naval warfare and maritime security, *The Journal of Defense Modeling and Simulation* (2024) 15485129241283056.
- [6] S. Bhat, I. Stenius, Hydrobatics: A review of trends, challenges and opportunities for efficient and agile underactuated auvs, in: 2018 IEEE/OES Autonomous Underwater Vehicle Workshop (AUV), IEEE, pp. 1–8.
- [7] K. D. Do, J. Pan, Control of ships and underwater vehicles: design for underactuated and nonlinear marine systems, Springer Science & Business Media, 2009.
- [8] L. Lapierre, D. Soetanto, Nonlinear path-following control of an auv, *Ocean engineering* 34 (2007) 1734–1744.
- [9] D. Belleter, M. A. Maghenem, C. Paliotta, K. Y. Pettersen, Observer based path following for underactuated marine vessels in the presence of ocean currents: A global approach, *Automatica* 100 (2019) 123–134.
- [10] T. I. Fossen, M. Breivik, R. Skjetne, Line-of-sight path following of underactuated marine craft, *IFAC proceedings volumes* 36 (2003) 211–216.
- [11] M. Breivik, T. I. Fossen, Principles of guidance-based path following in 2d and 3d, in: Proceedings of the 44th IEEE Conference on Decision and Control, IEEE, pp. 627–634.
- [12] T. I. Fossen, K. Y. Pettersen, On uniform semiglobal exponential stability (usges) of proportional line-of-sight guidance laws, *Automatica* 50 (2014) 2912–2917.
- [13] A. Pavlov, H. Nordahl, M. Breivik, Mpc-based optimal path following for underactuated vessels, *IFAC Proceedings Volumes* 42 (2009) 340–345.
- [14] A. M. Lekkas, T. I. Fossen, A time-varying lookahead distance guidance law for path following, *IFAC Proceedings Volumes* 45 (2012) 398–403.
- [15] W. Caharija, K. Y. Pettersen, M. Bibuli, P. Calado, E. Zereik, J. Braga, J. T. Gravdahl, A. J. Sørensen, M. Milovanović, G. Bruzzone, Integral line-of-sight guidance and control of underactuated marine vehicles: Theory, simulations, and experiments, *IEEE Transactions on Control Systems Technology* 24 (2016) 1623–1642.
- [16] Y. Zhang, S. Li, W. Wang, S. Wang, R. Mu, Three-dimensional path following control of underactuated autonomous underwater vehicles with nonzero roll dynamics: A novel line-of-sight-guided approach, *International Journal of Robust and Nonlinear Control* 34 (2024) 4959–4977.
- [17] J. Nie, X. Lin, Improved adaptive integral line-of-sight guidance law and adaptive fuzzy path following control for underactuated msv, *ISA transactions* 94 (2019) 151–163.
- [18] T. I. Fossen, A. P. Aguiar, A uniform semiglobal exponential stable adaptive line-of-sight (alos) guidance law for 3-d path following, *Automatica* 163 (2024) 111556.
- [19] B. S. Kim, A. J. Calise, R. J. Sattigeri, Adaptive, integrated guidance and control design for line-of-sight-based formation flight, *Journal of Guidance, Control, and Dynamics* 30 (2007) 1386–1399.
- [20] L. Liu, D. Wang, Z. Peng, Eso-based line-of-sight guidance law for path following of underactuated marine surface vehicles with exact sideslip compensation, *IEEE Journal of Oceanic Engineering* 42 (2016) 477–487.
- [21] H. Xu, T. I. Fossen, C. G. Soares, Uniformly semiglobally exponential stability of vector field guidance law and autopilot for path-following, *European Journal of Control* 53 (2020) 88–97.
- [22] W. Caharija, K. Y. Pettersen, P. Calado, J. Braga, A comparison between the ilos guidance and the vector field guidance, *IFAC-PapersOnLine* 48 (2015) 89–94.
- [23] N. Gu, D. Wang, Z. Peng, J. Wang, Q.-L. Han, Advances in line-of-sight guidance for path following of autonomous marine vehicles: An overview, *IEEE Transactions on Systems, Man, and Cybernetics: Systems* 53 (2022) 12–28.
- [24] S. P. Berge, K. Ohtsu, T. I. Fossen, Nonlinear control of ships minimizing the position tracking errors, *IFAC Proceedings Volumes* 31 (1998) 129–134.
- [25] F. Alonge, F. D’Ippolito, F. M. Raimondi, Trajectory tracking of underactuated underwater vehicles, in: Proceedings of the 40th IEEE conference on decision and control (Cat. No. 01CH37228), volume 5, IEEE, pp. 4421–4426.
- [26] L. Degorre, T. I. Fossen, O. Chocron, E. Delaleau, A model-based kinematic guidance method for control of underactuated autonomous underwater vehicles, *Control Engineering Practice* 152 (2024) 106068.
- [27] J. Matouš, C. Paliotta, K. Y. Pettersen, D. Varagnolo, The hand position concept for control of underactuated underwater vehicles, *IEEE Transactions on Control Systems Technology* (2024).
- [28] C. Paliotta, E. Lefeber, K. Y. Pettersen, J. Pinto, M. Costa, et al., Trajectory tracking and path following for underactuated marine vehicles, *IEEE Transactions on Control Systems Technology* 27 (2018) 1423–1437.
- [29] L. Degorre, T. I. Fossen, E. Delaleau, O. Chocron, A virtual reference point kinematic guidance law for 3-d path-following of autonomous underwater vehicles, *IEEE Access* (2024).
- [30] J. Matouš, K. Y. Pettersen, D. Varagnolo, C. Paliotta, E.-L. Ruud, Adaptive hand position for underactuated underwater vehicles, *IEEE Journal of Oceanic Engineering* (2025).
- [31] T. I. Fossen, Handbook of marine craft hydrodynamics and motion control, John Wiley & Sons, 2011.
- [32] K. Y. Pettersen, H. Nijmeijer, Underactuated ship tracking control: theory and experiments, *International Journal of Control* 74 (2001) 1435–1446.
- [33] L. Martinović, Ž. Zečević, M. Bibuli, M. Caccia, Đ. Nađ, Adaptive observer-based line-of-sight guidance law for path following of underactuated unmanned surface vehicle with sideslip compensation, *IEEE Access* (2024).
- [34] G. Besançon, J. de León-Morales, O. Huerta-Guevara, On adaptive observers for state affine systems, *International journal of Control* 79 (2006) 581–591.
- [35] G. Besançon, G. Bornard, H. Hammouri, Observer synthesis for a class of nonlinear control systems, *European Journal of control* 2 (1996) 176–192.
- [36] R. Grandia, A. J. Taylor, A. Singletary, M. Hutter, A. D. Ames, Nonlinear model predictive control of robotic systems with control lyapunov functions, *arXiv preprint arXiv:2006.01229* (2020).
- [37] M. Menghini, S. Mallipeddi, P. Castaldi, L. De Marchi, Neuro adaptive integral sliding mode control based on composite learning for path following of underactuated underwater vehicle: Blucy, in: Conference Proceedings of iSCSS, volume 2024.
- [38] K. Y. Pettersen, O. Egeland, Time-varying exponential stabilization of the position and attitude of an underactuated autonomous underwater vehicle, *IEEE Transactions on Automatic Control* 44 (2002) 112–115.
- [39] H. K. Khalil, J. W. Grizzle, *Nonlinear systems*, volume 3, Prentice hall Upper Saddle River, NJ, 2002.
- [40] M. Menghini, S. Mallipeddi, L. De Marchi, P. Castaldi, Modelling and parameter identification of uuv blucy for control design: A benchmark model, *Ocean Engineering* 313 (2024) 119617.